Published online 3 September 2010 *Nucleic Acids Research, 2011, Vol. 39, No. 1* ***155–167***
doi:10.1093/nar/gkq766

Visualizing RAD51-mediated joint molecules: implications for recombination mechanism and the effect of sequence heterology

D. Ristic[1], R. Kanaar[1,2] and C. Wyman[1,2,*]

[1]Department of Cell Biology and Genetics, Cancer Genomics Center and [2]Department of Radiation Oncology, Erasmus MC, PO Box 2040, 3000 CA Rotterdam, The Netherlands

Received September 22, 2009; Revised August 5, 2010; Accepted August 11, 2010

ABSTRACT

The defining event in homologous recombination is the exchange of base-paired partners between a single-stranded (ss) DNA and a homologous duplex driven by recombinase proteins, such as human RAD51. To understand the mechanism of this essential genome maintenance event, we analyzed the structure of RAD51–DNA complexes representing strand exchange intermediates at nanometer resolution by scanning force microscopy. Joint molecules were formed between substrates with a defined ssDNA segment and homologous region on a double-stranded (ds) partner. We discovered and quantified several notable architectural features of RAD51 joint molecules. Each end of the RAD51-bound joints had a distinct structure. Using linear substrates, a 10-nt region of mispaired bases blocked extension of joint molecules in all examples observed, whereas 4 nt of heterology only partially blocked joint molecule extension. Joint molecules, including 10 nt of heterology, had paired DNA on either side of the heterologous substitution, indicating that pairing could initiate from the free 3′ end of ssDNA or from a region adjacent to the ss–ds junction. RAD51 filaments covering joint ss–dsDNA regions were more stable to disassembly than filaments covering dsDNA. We discuss how distinct structural features of RAD51-bound DNA joints can play important roles as recognition sites for proteins that facilitate and control strand exchange.

INTRODUCTION

Homologous recombination is an essential process underpinning replication and assuring genome maintenance. The defining mechanistic step of homologous recombination, exchange of base-paired partners between single-stranded (ss) DNA and its homolog within double-stranded (ds) DNA, is catalyzed by recombinase proteins such as human RAD51. Strand exchange is essentially a DNA rearrangement event catalyzed by a DNA-bound RAD51 filament. The arrangement of RAD51 in DNA bound filaments is coupled to adenosine triphosphates (ATP) binding and hydrolysis. The stand exchange reactions proceed from assembly of RAD51 filaments on ssDNA, to rearrangement of RAD51 filaments in a joint molecule complex, involving both ssDNA and a homologous sequence dsDNA, and finally disassembly of RAD51 from the dsDNA product. Here, we consider strand exchange as defined by this series of rearrangements of RAD51–DNA complexes.

The basic arrangement of DNA-bound recombinase filaments is symmetric and regular. As first determined for bacterial RecA, recombinases form a right-handed helical protein filaments around the right-handed DNA helix (1–3). ATP is bound between adjacent recombinase protomers assembled into filaments on DNA (4–6). This protein interface constitutes an ATPase active site. The status of the bound nucleotide cofactor correlates with differences in helical pitch (rise per helical turn) for both RecA and RAD51. ATP-bound filaments have a longer pitch (4) and are believed to be the forms active in strand exchange. ADP-bound filaments have a shorter pitch and are described as inactive in strand exchange (7). These recombinase filament characteristics were determined from static forms using methods that require a uniform structural population, such as crystalographic analysis or image reconstitution from EM preparations. However, dynamic interactions of RAD51 and DNA, resulting in structural variation, are critical for homologous recombination. The assembly, disassembly and changes in structure of RAD51 filaments have been defined more directly by single-molecule manipulation and imaging experiments (8–13).

Assembly of RAD51 filaments on ssDNA is necessarily a dynamic process and is required to form the active

*To whom correspondence should be addressed. Tel: +31 10 704 4337; Fax: +31 10 704 4743; Email: c.wyman@erasmusmc.nl

machinery of strand exchange. RAD51 filaments form by nucleation of protein on DNA then growth of the DNA-bound protein filament, both described best to involve RAD51 multimers (10,12,13). If RAD51 remains in the ATP-bound state (using non-hydrolyzable ATP analogs, ATPase transition state analogs or suppressing ATPase activity) filaments formed on ssDNA can be stable and regular (8,10,12,14–16). However, active ATP hydrolysis results in irregular and dynamic structures on ssDNA due to continuous RAD51 assembly, disassembly and likely rearrangements (8,10). Specifically, ATP-bound RAD51 nucleates rapidly on both ss and dsDNA. ATP hydrolysis triggers disassembly of RAD51 faster from ssDNA than from dsDNA (10,12).

The nucleation, growth and disassembly characteristics of RAD51 result in ssDNA bound by relatively short patches of continuous protein interspersed with free DNA. Thus, RAD51–ssDNA nucleoprotein filaments are notably dynamic and flexible (10). These dynamic interactions of RAD51 with ssDNA may be required to eventually assemble a continuous protein filament long enough to accomplish stand exchange. Alternatively, and the view we favor, the flexible and dynamic nature of the ssDNA–RAD51 complex may promote dynamic interactions with dsDNA that allow efficient identification of homology and strand exchange.

In productive strand exchange, RAD51 bound to the dsDNA heteroduplex is the product of the reaction. Subsequent steps of homologous recombination require disassembly of RAD51 filaments form this dsDNA product. RAD51 filaments on dsDNA can be regular and stable in an ATP-bound state (8–13,17). RAD51 filaments on dsDNA change conformation in conditions that likely represent an ADP-bound state (8,13). ATP hydrolysis clearly triggers disassembly of filaments from dsDNA (8–10,13,18). Disassembly occurs via release of protomers from filament ends (10). By analogy to RecA (19), ATP is likely hydrolyzed throughout the filament. Single-molecule manipulation combined with quantitative detection of fluorescently labeled RAD51 revealed that RAD51 disassociates in bursts of varying size (11). This is most easily explained by release of a terminal RAD51 protomer once it has hydrolyzed ATP along with any adjacent protomers that have already hydrolyzed ATP. In addition, RAD51 disassembly is sensitive to tension applied to the DNA (11), which can be explained if the external tension keeps DNA stretched as it is in RAD51 nucleoprotein filaments. Because dsDNA bound by RAD51 is stretched, release of this energy would help drive the strand exchange reaction forward, disfavoring RAD51 re-association with the dsDNA product.

A detailed picture describing the beginning and end (RAD51 assembly on ssDNA and disassembly from dsDNA) of strand exchange is rapidly emerging. The critical behavior of RAD51 during strand exchange has yet to be described. Here, we used scanning force microscopy (SFM) imaging to determine the architecture of RAD51–DNA complexes involved in strand exchange. We included defined heterologous sequences to determine the effect of this potential block to strand exchange on the architecture of the complexes. For instance, if strand exchange is blocked by heterology does this prevent joint molecule formation or otherwise influence the (local) structure of RAD51-bound joint DNA molecules? Specific distortions of the target dsDNA were defined, which may be recognized by accessory proteins needed for controlled and efficient homologous recombination. These new insights into RAD51 joint molecule filament structure provide valuable clues to the mechanism of DNA strand exchange and how it may be controlled and regulated.

MATERIALS AND METHODS

DNA substrates and proteins

Table of primers

Name	Sequence
URA3	GAAGGAAGAACGAAGGAAGGAGC
BIO5′	TTTCCCGGGGGGGCCCGGGTTCTATACTGTTGACCC SmaI SmaI
DR3	GGTCCCAAAATTTGTTTACTAAAA
DR5	CCCGGGAGCTCGAAGGAAGAACGAAGGAAGGAGC SacI
DR6	TTTCCCACGTAGTGGTATACACCCGCAGAGTACTGCA DraIII
SPH1A	GTCCGGATGCATGCTCCTGCAGGTTTTTGTTCTGTGC SphI
SPH1B	CGTAGTGCATGCAAAAAACGAAGATAAATCATGTCGA SphI
KPN	TTTCGCGGTACCCCCGGGTAATAACTGATATAAT KpnI
NHEA	TTGATCGCTAGCCTGCAGGTTTTTGTTCTGT NheI
NHEB	CGTAGAGCTAGCAACCGAAACGAAGATAAATCATG NheI
SPH+1A	CCGGATGCATGCTATTCCTGCAGGTTTTTGTTCTGTGC SphI
SPH+1B	CGAGTCGCATGCGTGGCCTGCAGGTTTTTGTTCTGTGC SphI
SPH+2	CGTAGTGCATGCAAACGAAGATAAATCATGTCGA SphI

DNA substrates

DNA with a 3′ ss overhang was made as follows: using the *URA3* gene from Saccharomyces *cerevisiae* as template DNA, an 810-bp polymerase chain reaction (PCR) fragment was produced using primer URA3 which was 5′ phosphorylated and primer BIO 5′ which was 5′ biotinylated. The PCR product was purified on a GFX^{TM} column (GE Healthcare) and incubated with 1 mg of streptavidin-coated magnetic beads (Dynabeads M-270, Invitrogen) for 2 h at 37°C in 400 µl of BW buffer (5 mM Tris–HCl pH 7.5, 0.5 mM EDTA, 1 M NaCl). Using a magnetic particle concentrator, the immobilized DNA was washed two times with 100 µl of BW buffer. Subsequently, the DNA was washed once with 100 µl of 1× λ exonuclease buffer (NEB). The DNA bound to the beads was made ss by λ exonuclease digestion of the strand with 5′ phosphate (5 U/µg DNA, NEB). The reaction was carried out at 37°C for 1 h. Immobilized ssDNA was washed with 100 µl of BW buffer. Subsequently, the DNA was washed once with 100 µl of

1× Sequenase buffer (USB) and hybridized with oligonucleotide primer DR3, which anneals at position 290–313 along the ss PCR product. Primer DR3 was extended for 30 min at 37°C in a reaction containing Sequenase™ DNA polymerase Version 2.0 (USB) in 100 µl of 1× Sequenase buffer supplemented with 200 mM dNTPs. The resulting DNA with 505 bp ds region and 289-nt 3′ overhang was washed with 100 µl of BW buffer, released from streptavidin-coated magnetic beads by digestion with Sma I (ROCHE) and purified on a GFX™ column.

Three'-tailed DNA with the same ds and ss arrangement but including a 4-or 10-bp heterologous substitution in the middle of pairing region, was made by using plasmids with these defined heterologous substitutions as template DNA in PCR reactions as described above. The rest of the protocol was as described above.

Three'-tailed DNA with 10 bp heterologous addition at the 3′ ss-end was made as follows: using the *URA3* gene from *S. cerevisiae* as template DNA, an 820 bp PCR fragment was produced using primer 3′BLOCK which was 5′ phosphorylated and primer Bio 5′ which was 5′ biotinylated. The rest of the protocol was as described above.

Vector pBlueScriptKS-(Stratagene) was used for cloning heterologous sequences into the *URA3* gene. Fragments of the URA3 gene were amplified by PCR using primers that introduced unique restriction recognition sites and regions of heterology. The sequence of all constructs was confirmed by restriction enzyme analysis and DNA sequencing.

Plasmid DR2 (3020 bp) was made by ligating a fragment consisting of the first 466 bp of the URA3 gene between Sac I and Dra III sites of pBlueScriptKS-(Stratagene). Plasmid DR3 (3030 bp) was made by ligating a fragment consisting of the first 466 bp of the *URA3* gene between SacI and DraIII sites of pBlueScriptKS-(Stratagene). The 10 bp heterologous sequence was introduced between nt position 121 and 122 of the *URA3* gene. Plasmids DR4, DR5 and DR6 (3901 bp) were made by ligating the 1021 bp *URA3* gene between SacI and KpnI sites of pBlueScriptKS-(Stratagene). The 10-bp heterologous sequences were introduced between nt position 121 and 122 of the *URA3* gene.

All supercoiled plasmids, used as recombination partners, were prepared by detergent lysis and purified by CsCl gradient equilibrium sedimentation.

Linear DNAs used as recombination partners were produced by digestion of plasmids with Xmn I (NEB) and purifed on a GFX™ column. The arrangements of homologies are schematically presented at Figures 1A and 4A. A complete description of how the DNA substrates were produced can be found in Supplementary Data.

Proteins

RAD51 purification. The human RAD51 protein was expressed in *Escherichia coli* and purified as previously described (9). Briefly, cells were lysed in high salt. The clarified lysate was treated with polyethylenimine. After a second clarification, RAD51 was recovered by $(NH_4)_2SO_4$ salting-out and the resuspended pellet was purified by heparin-sepharose chromatography followed by MonoQ chromatography. The protein eluted from MonoQ was dialyzed against 300 mM KCl, 20 HEPES–NaOH (pH 7.8), 1 mM EDTA, 2 mM DTT and 10% glycerol and stored at 80°C.

Scanning force microscopy

Human RAD51–DNA complexes were formed in 10 µl reactions containing 7.5 µM DNA (concentration in nt/bp, adjusted concentration to indicate nt or bp along the DNA such that RAD51 concentration is sufficient to cover the entire DNA fragment at one monomer per 3 nt or bp), 2.5 µM RAD51, 25 mM HEPES-KOH (pH 7.5), 5 mM $CaCl_2$, 2 mM ATP, 30 mM KCl. Reactions were incubated at 37°C for 30 min and than placed on ice.

Reactions were diluted 10-fold in deposition buffer (10 mM HEPES-KOH pH 7.5, 10 mM $MgCl_2$) and deposited on freshly cleaved mica. After 20 s, the mica was washed with water and dried in a stream of filtered air.

Joint molecules were formed and deposited for imaging as follows: one-tenth of the volume of the filament formation reaction mixture was mixed with 0.75 µM homologous circular or linear DNA (concentration in bp), in 25 mM HEPES-KOH (pH 7.5), 5 mM $CaCl_2$, 2 mM ATP, 30 mM KCl. After 30 min at 37°C, 100 mM $(NH_4)_2SO_4$ (final concentration) was added and incubated for 10 min at 37°C. The reaction mixture was transferred onto freshly cleaved mica and after 20 s washed with 10 mM HEPES-KOH (pH 7.5), 30 mM KCl. The excess buffer was removed and replaced with a buffer containing 10 mM HEPES-KOH (pH 7.5), 10 mM $MgCl_2$ in order for DNA to attach to mica. After 5 s the mica was washed with water and exposed to a stream of filtered air. Note that the deposition onto mica in $MgCl_2$ containing buffers would not affect the observed structure of the RAD51–DNA complexes formed in the presence of $CaCl_2$. Based on the RAD51 filament disassembly rates measured in solution upon change from $MgCl_2$ to $CaCl_2$ (10), filaments of the length used here exposed to $MgCl_2$ for 5 s would maximally loose nine monomers due to dissociation along the joint molecule regions, which would not noticeably change their appearance in SFM images. In addition, disassembly of RAD51 filaments triggered on mica as done here is much slower and therefore a 5-s exposure is even less likely to influence filament appearance (8).

To study complex disassembly on mica, joint molecules were formed as described above including treatment with $(NH_4)_2SO_4$. Reaction mixtures were deposited on mica and washed with 10 mM HEPES-KOH (pH 7.5), 30 mM KCl. The excess buffer was removed and replaced with a buffer containing 25 mM HEPES-KOH (pH 7.5), 5 mM $MgCl_2$, 2 mM ATP and 30 mM KCl. The joint molecules were incubated on mica at about 19°C (RT) for 10 min and then washed with water and dried in a stream of filtered air.

Images were obtained with a NanoScope IIIa or NanoScope IV SFM (Digital Instruments; Santa Barbara, CA, USA) operating in tapping mode in air with a type E scanner. Uncoated silicon Pointprobe tips

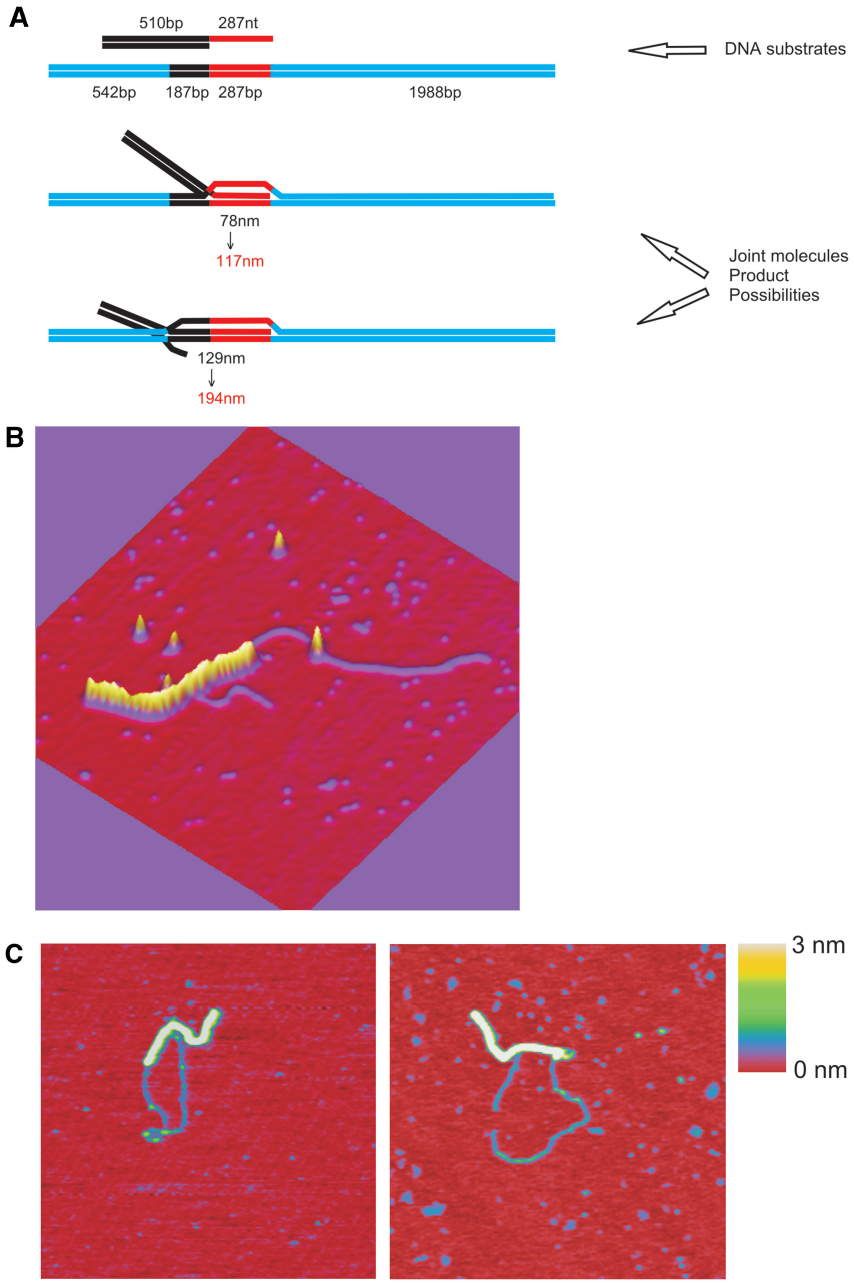

Figure 1. DNA substrates and joint molecule products. (**A**) Diagram of DNA substrates (top) and possible joint molecules (middle and bottom). The 3020 bp dsDNA partner was pDR2 circular or linearized by Xmn I. The homologous sequences are represented by the same color, red or black. The lengths of different regions of the DNA substrates are indicated in base pairs (bp) or nucleotides (nt). The theoretical lengths of the homologous region are indicated in nanometers (nm), the shorter length corresponds to B-form DNA and the longer length corresponds to the indicated region of nt/bp bound by a RAD51 filament that extends DNA to 1.4 times B-form length. (**B**) Three-dimensional view of joint molecule formed with linear dsDNA and imaged by SFM. (**C**) SFM images showing joint molecules formed with circular (left) and linear (right) dsDNA. The circular DNA is the same 3020 bp substrate illustrated in A but not linearized. The images are $1 \times 1\,\mu m$ and the *z*-dimension is indicated by color as shown on the bar at the right.

were type NHC-W, resonance frequency 310–372 kHz, force constant $C = 29.0–52.0\,N/m$, (Nanosensors supplied by Veeco Instruments, Europe).

The length measurements were done from NanoScope images imported into IMAGE SXM 1.62 (NIH-IMAGE version modified by Steve Barrett, Surface Science Research Centre, Univ. of Liverpool, Liverpool, U.K.). The contours of filaments and DNA were traced manually. The height measurements along filaments were done from NanoScope images imported into WSxM4.0 Develop 9.2 (Nanotec Electronica S.L.). The contours of filaments and DNA were traced manually.

Analysis of strand exchange efficiency

All reaction steps were carried out at 37°C. ^{32}P-labeled 3′-tailed DNA (7.5 μM in bp/nt, adjusted concentration to indicate nt or bp along the DNA such that RAD51

concentration is sufficient to cover the entire DNA fragment at one monomer per 3 nt or bp) was incubated with RAD51 (2.5 μM) in 10 μl reactions mixtures containing 25 mM HEPES-KOH (pH 7.5), 5 mM $CaCl_2$, 2 mM ATP, 30 mM KCl. After 30 min the indicated supercoiled plasmid (36 μM) was added and the reaction continued for 30 min. The reactions were stopped by addition of SDS (0.5%) and proteinase K (0.5 mg/ml) and incubating for 10 min. The DNA was resolved by electrophoresis through a 0.9% agarose gel in TAE buffer (40 mM TRIS pH 7.4, 0.5 mM EDTA). The electrophoresis was carried out at 4°C for 8 h at 1.9 V/cm. The gels were dried and the ^{32}P-labeled DNA was visualized and quantified using a phosphorimager.

RESULTS

dsDNA in RAD51 joint molecules is extended and specifically distorted at joint junctions

To analyze RAD51-catalyzed joint molecule formation by SFM we made DNA substrates with distinct structure and defined regions of homology (Figure 1A). RAD51 was first incubated with 3′ ss-tailed linear DNA to assemble nucleoprotein filaments. The strand exchange reaction was initiated by addition of dsDNA, either linear or circular (supercoiled), including a region homologous to the ssDNA portion of the other DNA molecule. Joint molecules formed readily with both circular and linear dsDNAs (Figure 1B and C), although less efficiently with linear DNA. In these strand exchange reactions we used ATP as nucleotide cofactor and Ca^{2+} as divalent cation, conditions that greatly suppress ATP hydrolysis and stimulate *in vitro* strand exchange by promoting accumulation of stable RAD51–DNA complexes (9–11,13,15). We determined the position of strand pairing and the extension of DNA involved in strand pairing. All observed joint molecules with the linear dsDNA partner had the same arrangement (Figure 1B and C, right) where the polarity of pairing was consistent with the sequence and position of homologous segments. The contour length of dsDNA in joint molecules was measured by tracing a path along the DNA and through the highest points of the paired region of joint molecules. This was compared to the contour length of linear dsDNA alone measured in the same manner. The measured contour lengths (Table 1) revealed that the position of ss–ds DNA pairing corresponded to the position of homology. The length of the upstream dsDNA (205 ± 40 nm, $n = 50$) indicated that only the 3′ ss part of the RAD51-coated DNA participated in homologous pairing, and as expected the potential four-stranded joint molecule (including homologous sequence indicated in black in Figure 1A) did not form. The length of the joint region (105 ± 40 nm, $n = 50$) indicated that the 289 bp of DNA in the homologous ds exchange partner was extended, ~1.4 times compared to B form, to the same extent as dsDNA alone bound by RAD51, previously characterized in similar SFM imaging (8).

The target dsDNA was notably and consistently distorted in the joint molecule complexes. To quantify these DNA distortion we measured the bend angle at three defined positions; designated (α) between the filament and dsDNA with an apex at the 3′ end (with respect to the invading ssDNA) of the paired regions, (β) between the filament and dsDNA with an apex at the 5′end (with respect to the invading ssDNA) of the paired region and (γ) along the nucleoprotein filament with an apex at the point where the dsDNA exits (Figure 2). By convention, bend angles are expressed as absolute value of the difference between measured angle and 180°. The distributions of these bend angles are shown in Figure 2. As expected, the nucleoprotein filament was rather rigid, expressed in the γ angle with an average of 0° and a narrow distribution. Thus, there is no distortion of the RAD51 filament at the position where the dsDNA exits. The junction between the 3′ end of the invading ssDNA, and the dsDNA does not have a defined arrangement as evident in the wide distribution of angle α (average 60 ± 33° $n = 60$) From this analysis the width of the distribution or standard deviation of the angle measurements indicates flexibility of the structure (20). The flexibility of DNA alone deposited under these conditions results in bend angle standard deviations of about 20°. The larger standard deviation of the angle α indicated flexible greater than DNA alone, likely due to distortion of the normal double helix. In contrast, dsDNA at the other junction of the nucleoprotein filament, the β angle, where homologous pairing ends at the 5′end of the invading ssDNA was bent sharply at 90° with a narrow distribution (average 82 ± 19° $n = 60$). Thus, our experiments revealed that there are distinct structural features at each end of the RAD51-bound DNA joints.

Table 1. Measured length of different segments in RAD51 joint molecules

	Upstream DNA	Paired region	Downstream DNA	Total DNA
Measured length in nm	205 ± 40	105 ± 40	577 ± 57	882 ± 72
Corresponding length in bp	733	(289)	1998	3020

All nm lengths are average ± standard deviation, $n = 50$.
Total DNA is the contour length of the 3 kbp dsDNA measured from the same SFM images. Given that 882 nm equals the whole 3020 bp, then 205 and 577 nm correspond to the length of DNA on each side of the paired region shown in the middle diagram of Figure 1A, which are 733 and 1998 bp, respectively. The remaining dsDNA, 289 bp in parenthesis to indicate it was not directly measured but calculated from the total length minus the two measured segments, must be included in the paired region, where the 105-nm length indicates extension to ~1.4 times that of B-form DNA.

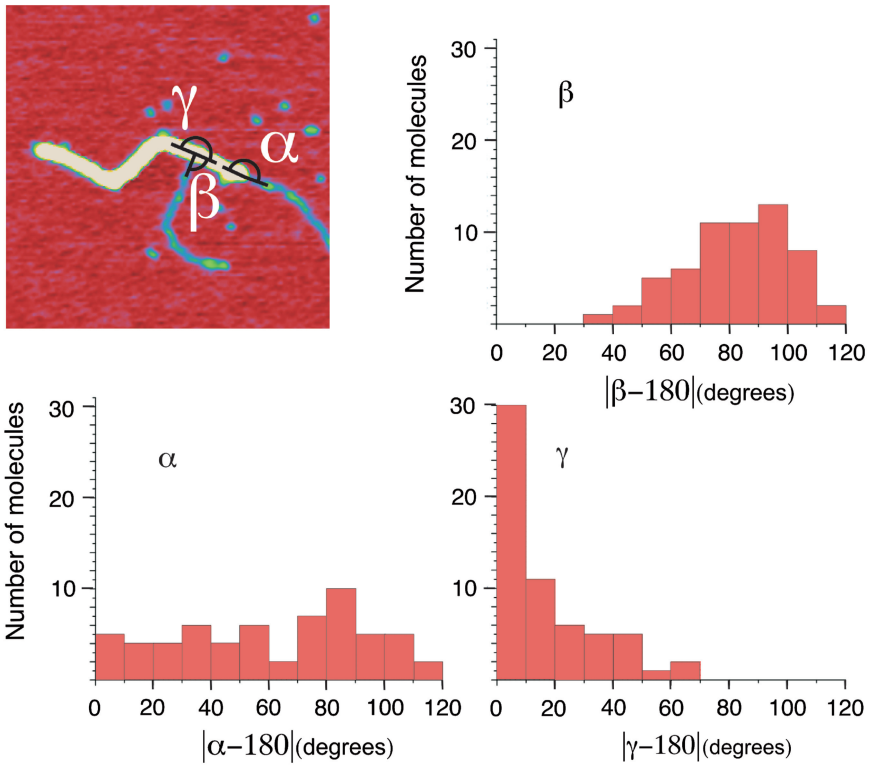

Figure 2. The dsDNA partner is distorted in joint molecules. SFM image of a joint molecule indicating positions where bend angles were measured (top left). Angle α is between the dsDNA and the 3′-end of the RAD51 filament with the apex at their junction. Angle β is between the dsDNA and the RAD51 filament corresponding to the 5′ end of the ssDNA with an apex at their junction. Angle γ is along the RAD51 filament with an apex at the junction with dsDNA, same position as the apex of angle β. All angles are expressed as absolute value of the difference between measured angle and 180° and their distribution is plotted in histograms (top right and bottom). Histograms show the distribution of bend angles at the three positions measured for a total of 60 joint molecules.

RAD51 filaments coating joined DNA segments were less regular but more stable to disassociation than RAD51 filaments on dsDNA

In the joint molecules imaged here, RAD51 covered both the non-homologous dsDNA and the segment where ss and homologous dsDNA were paired Thus, we could directly compare these two types of filaments. RAD51 forms regular and stable filaments with elongated dsDNA under conditions that enhance accumulation of recombination products *in vitro* (8–10,15). The common feature of these conditions is that they maintain RAD51 in an ATP-bound conformation and prevent protein disassociation. ATP hydrolysis by RAD51 results in protein release and filaments on dsDNA that appear irregular in SFM (8–10,18). This irregular appearance suggests that the filaments are dynamic with subunits binding and disassociating. We compared filament structure along the unpaired and paired segments. Filaments in these regions did not differ greatly in appearance. Filament regularity was quantified by measuring the height profile along the filament axis. The filament contours were traced manually (Figure 3A and B) and cumulative heights measured for all positions along the various segments were plotted in histograms (Figure 3C). Heights along the non-paired region of filaments, i.e. RAD51-coated dsDNA, were the most regular as evident by the single-peak distribution (Figure 3C, top right). The height profile of RAD51 filament covering the paired region indicated more irregularity, with cumulative height measurements distributed over a larger range of values (Figure 3C, top left). Lower positions, which indicate discontinuities or gaps in the protein filament, were more prevalent in the RAD51-coated joined regions compared to RAD51-coated dsDNA. The more irregular height profile of the paired regions is consistent with strand exchange involving dynamic rearrangements of protein in the filaments.

We have previously demonstrated disassembly of RAD51–DNA filaments immobilized on mica by incubating with buffer that allows ATP hydrolysis (8). We used this method here to assess differences in stability of RAD51 filaments on dsDNA compared to RAD51 filaments on paired DNA. Joint molecules were formed in the presence of ATP and Ca^{2+} as before, conditions that strongly suppress the ATPase activity of RAD51 (15). After addition of $(NH_4)_2SO_4$ and deposition onto mica, the buffer was replaced with one containing ATP and Mg^{2+}. The joint molecules were incubated on mica in this buffer for 10 min before visualization. Due to hydrolysis of ATP, RAD51 monomers dissociate from DNA (10,11), resulting in irregular appearance of the filaments (8). As seen in Figure 3B, ATP hydrolysis by RAD51 caused disorder in the nucleoprotein filament that was more pronounced in the non-paired regions. Before triggering ATP hydrolysis the height distribution for the

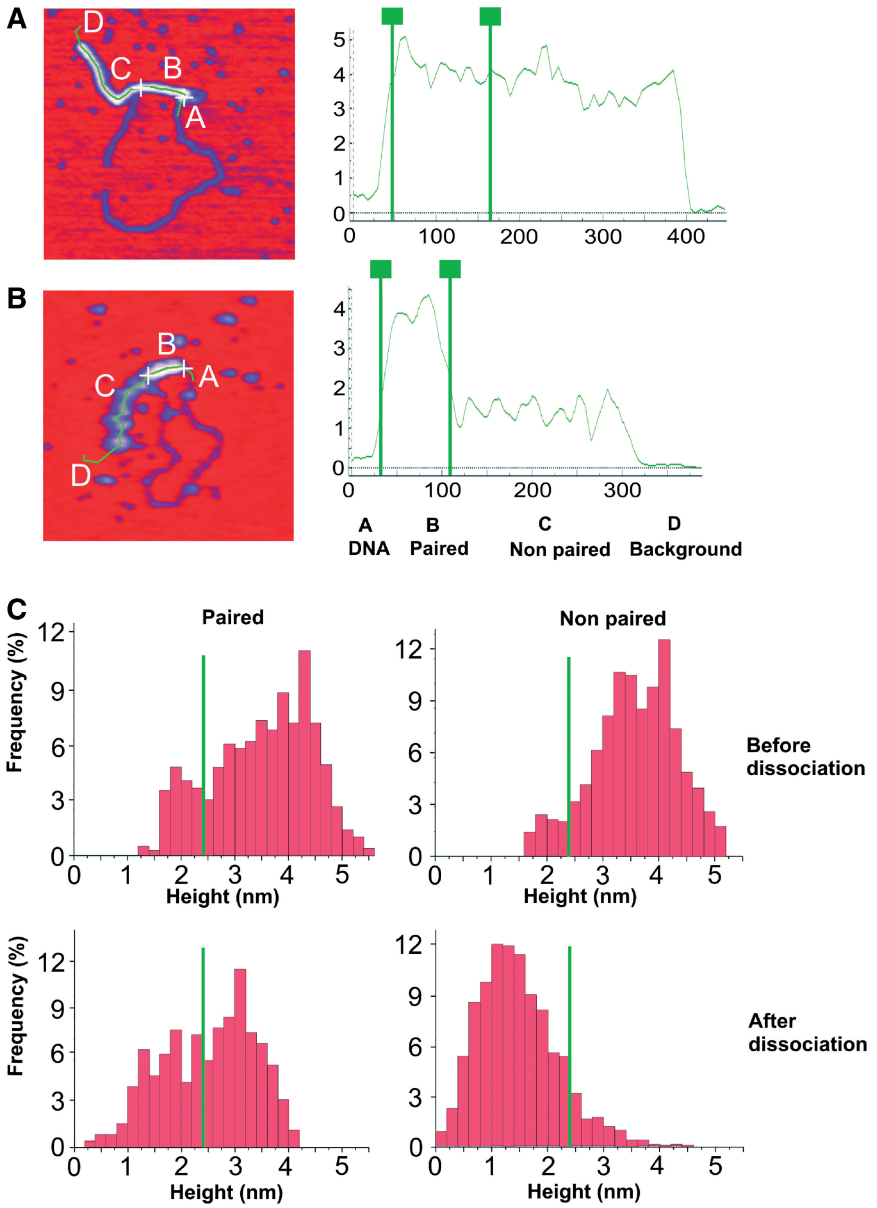

Figure 3. Comparing architecture and stability of RAD51 filaments along the paired and unpaired segments of joint molecules. Filament structure and stability were assessed by measuring height profiles along filaments, either before (**A**) or after partial dissociation (**B**). The contours were traced manually (A and B) along the path indicated on the images and displayed as profiles to the right with the different regions indicated as A = DNA, B = filament over paired regions, C = filament over unpaired dsDNA and D = mica surface background. Cumulative height measurements for all position along the indicted regions, from 50 joint molecules for the 'before dissociation' condition and 40 joint molecules for the 'after dissociation' condition, are plotted in histograms. The histograms show the percentage of positions having different heights (**C**). The cutoff value of 2.4 nm, chosen as an obvious separation in the distributions before dissociation, is indicated [green line in (C)].

paired regions included very few measurements lower than 2.4 nm (Figure 3C), indicating fairly continuous protein coverage. This value of 2.4 nm was chosen as a cutoff, to indicate loss of protein from the 4-nm high filaments, and used to describe the extent of filament disassembly. By these criteria, the paired regions were much more stable to disassembly than the unpaired regions. Before ATP hydrolysis 92.2% of the positions along the RAD51-coated dsDNA were >2.4 nm, which reduced to 9.8% after ATP hydrolysis (Figure 3C right, top versus bottom). This indicates that ATP hydrolysis triggers extensive disassembly of RAD51 from dsDNA as observed before (8–10,13). However, RAD51 filaments coating the paired DNA region appears more stable after ATP hydrolysis. Although less regular before ATP hydrolysis, as mentioned above, with 83.5% of the positions >2.4 nm this decreased to 56.7% after ATP hydrolysis (Figure 3C left, top versus bottom). Thus, in this assay we observed impaired release of RAD51 from joined DNA regions compared to dsDNA.

Effect of sequence heterology on joint molecule architecture

Homologous recombination is carefully controlled to maintain genome stability yet allow efficient

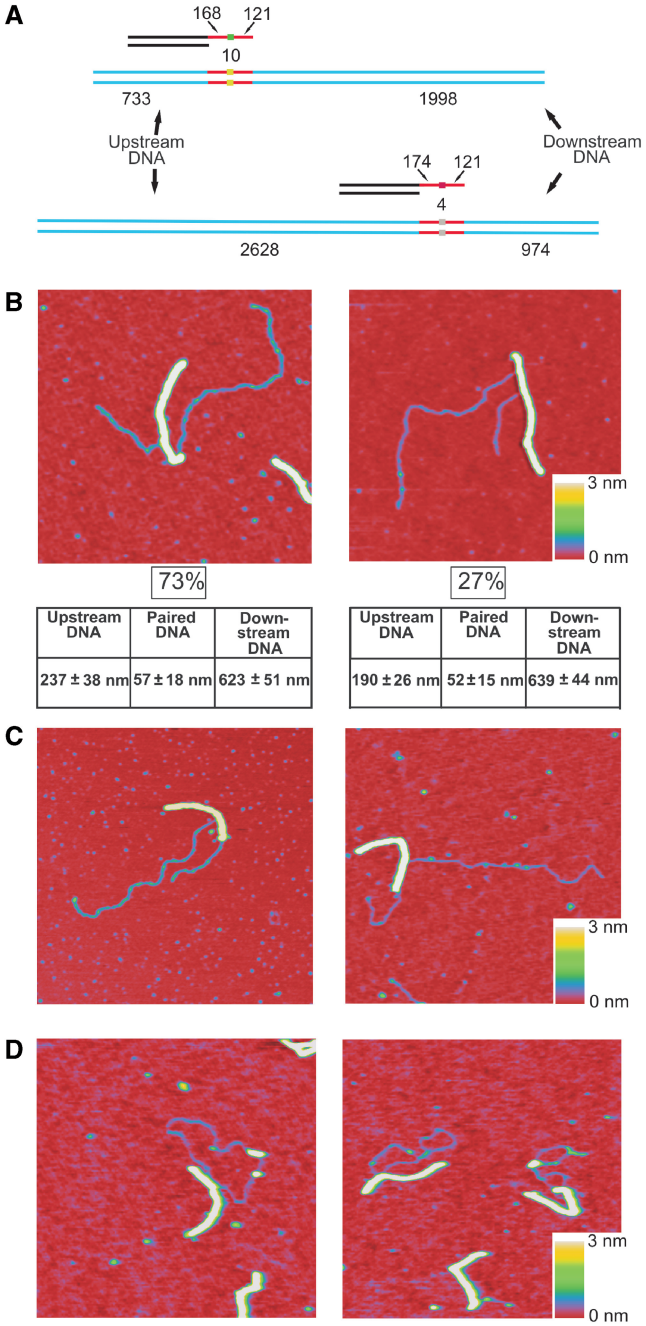

Figure 4. Effect of heterologous substitutions on joint molecule architecture. (**A**) Diagram of DNA substrates. The boxes in different color represent heterologous sequence substitutions. A 10-nt (top cartoon) or 4-nt (bottom cartoon) heterologous substitution was placed near the center of the ss recombination partner. The sequence of dsDNA was changed at the same positions to keep strand exchange in register. (**B**) SFM images of two types of joint molecules formed by DNA substrates with a 10-nt substitution near the center of the pairing region and linear plasmid pDR3 diagramed in (A) top. Both images are 0.75×0.75 μm. The percentage of joint molecules paired 3′ of the heterology (left) or 5′ of the heterology (right) is indicated below the image. The length of different regions was measured and listed in the tables for both type of structures ($n = 40$ for 3′-pairing, left and $n = 15$ for 5′ pairing, right). (**C**) SFM images of joint molecules formed by DNA substrates with a 4-nt substitution near the center of pairing region and linear plasmid pDR6 as diagramed at the bottom of (A). The paired region often extended past the homology and varied in length (50–100 nm, average 69 ± 24 nm, $n = 25$. The length of the unpaired regions varied accordingly). Images are 1×1 μm and the z-dimension is indicated by color as shown on the bar at the right. (**D**) SFM images of joint molecules formed by DNA substrates with a 10-nt heterologous substitution near the center of the pairing region and circular plasmid pDR4. Both images show joint molecules with the 3′ (shorter) end of the filament extending away and unpaired with the dsDNA partner. The right image has in addition an example of a fully paired joint molecule. Both images are 1×1 μm.

recombination between similar non-identical sequences. The degree to which sequence mismatches block strand exchange determines the fidelity of homologous recombination. In order to understand the stage of homologous recombination at which sequence fidelity is assessed we determined the effect of heterologous sequence substitutions on joint molecule formation and architecture. Either 4 or 10 nt near the center of the ss recombination partner was changed so that it was no longer homologous to the dsDNA recombination partner (Figure 4A). Joint molecule extension using linear dsDNA was apparently completely blocked by 10 bp of heterology positioned in the middle of the homologous sequences. Of 55 joint molecules observed using this ss partner all included pairing only up to the position of the heterologous substitution, the length of the paired region was about 50 nm compared to the 100-nm-long regions when all 289 nt/bp are paired (Figure 4B). Interestingly, pairing on either side of the heterologous substitution was observed. The majority of joint molecules, 73% (40 of 55 total), were paired over half of the ssDNA starting from the 3′ end, determined by measuring the length of the upstream dsDNA which included unpaired homologous sequences and the length of the unpaired filament which was longer (Figure 4B, left). The rest, 27% (15 of 55 total), did not include the 3′ end of the ssDNA in the joined region and were paired over the half of the homology between the ss–ds junction and the heterologous substitution, determined by measuring the length of the downstream dsDNA which included unpaired homologous sequences and clearly observing 50 nm or more of the filament 3′ end unpaired and extending away from the dsDNA (Figure 4B, right). The 3′ filament ends extending beyond the position of heterology were quantifiably different from the filament extensions beyond the 3′ end seen occasional in fully homologous pairing (Figure 1C, right). The occasional filament extensions seen with homologous substrates were short, about 10 nm, and not coupled with decreased length of the paired region or increased length of the unpaired dsDNA. The measured contour lengths of dsDNA (upstream and downstream of the joined region) and filament segments confirmed that only half of the ssDNA was paired, and that pairing occurred at the position of homology in the dsDNA for both types of joint molecules.

To test the influence of supercoiling on joint molecule extension at heterology, we used the circular supercoiled plasmid as a substrate in the reaction with the 10-nt heterologous substitution. In this case, the position of pairing cannot be determined as there is no landmark end of the dsDNA partner for measurements. However, we could accurately measure the length of the paired segment and

observe the presence or not of a free 3′ unpaired filament end. Using supercoiled circular DNA, the 10-nt heterologous substitution impaired but did not completely stop joint molecule extension. About 42% (48 of 114) of the joint molecules had a paired regions 60 nm long or less, indicating pairing only on one side of the heterology. The remaining 57% (66 of 114) had paired regions between 60 and 100 nm, indicating the paired region incorporated the heterology and extended beyond this position. Here also 24% ($n = 212$) of the partially paired joint molecules had unpaired regions at the 3′ end of the filament (Figure 4D), indicating that stable joint molecule formation did not require pairing of a 3′ homologous end.

To test whether homology at the 3′ end of the ssDNA partner was needed for joint molecule formation we placed a 10-nt heterologous sequence at the 3′ terminus of the ssDNA. Using this substrate we observed joint molecules with frequency and structure comparable to those obtained with the completely homologous substrate (images essentially the same as Figure 1B and C, data not shown). Thus, we conclude that homologous sequences at the 3′ terminus are not required for joint molecule formation.

Joint molecule extension was only partially blocked by 4 nt of heterologous sequence in the middle of ssDNA partner (as diagramed in Figure 4A, bottom). Using this substrate with 4 nt of heterology and linear dsDNA, 64% ($n = 25$) had paired DNA regions measuring 60–100 nm, indicating they had passed the heterologous sequence (Figure 4C, right). The remaining 36% of the joint molecules had paired regions that stopped at the position of heterology (50–60 nm, Figure 4C, left). Of the joint molecules including heterology in the joined region, only approximately one-third had paired along the complete homologous sequences (paired regions ~100 nm). The joint molecules where heterology was not completely bypassed also include either pairing from the 3′end of the ssDNA or from the ss-ds junction (based on the measured lengths of upstream or downstream dsDNA and arrangement of the unpaired filament, extending away from dsDNA at the 3′end in about 1/3 of the complexes observed), in approximately the same ratio as observed with the 10-bp heterologous substitution (Figure 4B and C left, data not shown). There was no obvious distortion or discontinuity in the RAD51 filament at the position of the heterologous sequence.

Strand exchange in joint molecules and effect of heterology on efficiency

To test if the joint molecules we observe have undergone strand exchange and to quantify the effect of heterologous sequence blocks on strand exchange efficiency we analyzed the products of RAD51-catalyzed joint molecule formation by agarose gel electrophoresis. Reaction products formed as for SFM imaging were deproteinized and resolved by agarose gel electrophoresis. DNA molecules that have undergone strand exchange remain associated after deproteinization (21) and can be detected based on their electrophoretic mobility. As expected, strand exchange was most efficient with completely homologous substrate; 12% of the linear DNA substrate was incorporated into joint molecules resistant to deproteinization. Strand exchange was less efficient with DNA substrates including a heterologous substitution; 9% of linear DNA with a 10-nt heterologous substitution at the 3′ end was incorporated into joint molecule product and 8% product was observed for substrates with either a 4- or 10-nt heterologous substitution in the middle of the ssDNA region of homology. Only one type of joint molecule was detected in reactions using completely homologous ssDNA substrate or ssDNA with the 10 nt of heterology at the 3′ end (Figure 5, upper band labeled JM) consistent with strand exchange along the entire homologous region. In the reactions using substrates with the central 4- or 10-nt heterologous substitution, two types of joint molecules with different electrophoretic mobility were resolved (Figure 5 bands labeled JM). Here, the 8% joint molecule product was the sum of these two resolved products (6% upper band + 2% lower band Figure 5).

Two different arrangements of joint molecules were observed in SFM imaging when ssDNA with central heterology was used. The ratio of joint molecules paired either 3′ or 5′ of the heterology (~3:1) seen in SFM images (Figure 4B) matched the ratio of the strand exchange products detected with different mobility in this gel assay. To determine if the two bands on the gel could represent the two types of joint molecules visualized by SFM we used a restriction enzyme protection assay. After joint molecules were formed, but before deproteinization, they were incubated with Sph I. This will linearize the circular DNA substrate only if the SphI recognition sequence, located 3′ (with respect to the ssDNA partner) in the heterology, is not included in the RAD51-bound joint molecule. Two possible arrangements for joint molecules susceptible to SphI cleavage are shown in Figure 5B, lower cartoons. Joint molecules resistant to SphI cleavage would have RAD51 bound as shown in Figure 5B top cartoons. After digestion with SphI only the joint molecules migrating as the lower band in the gel were diminished (Figure 5B, note that the linearized joint molecules undergo branch migration and are not detected in this gel assay). This confirms that the joint molecules in this band did not have RAD51 covered paired DNA at the 3′ side of the heterology. This gel assay was consistent with strand exchange occurring either 3′ or 5′ of the heterology with the same proportions as seen in SFM imaging.

DISCUSSION

We have revealed the structure of RAD51 joint molecule intermediates at nanometer resolution. This visualization identified distinct structural elements, showed the relative stability of bound recombinase and the consequences of encountering heterology. Interaction of RAD51-coated ssDNA was observed at the homologous region of dsDNA only. We did not observe any interactions with non-homologous dsDNA that would have indicated homology search. Interactions between RAD51-coated

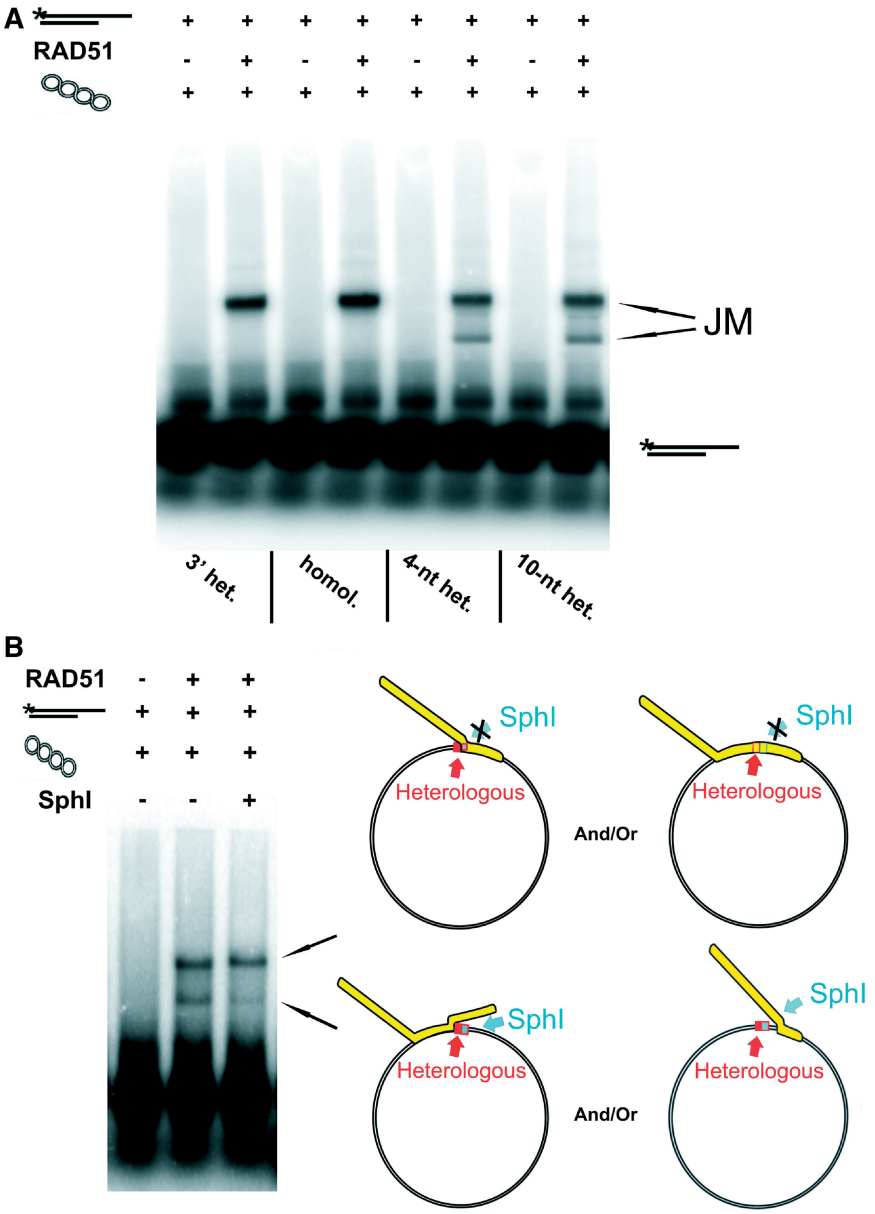

Figure 5. Effect of heterology on efficiency of strand exchange. Joint molecules formed between the radiolabeled 3′-ss-tailed dsDNA (* indicates 5′ radiolabeled phosphate) and supercoiled circular dsDNA substrates, as for SFM, were deproteinized and resolved by agarose gel electrophoresis. (**A**) The joint molecules formed between DNA partners with or without heterologous substitutions (indicated below). The positions of radiolabeled substrate and joint molecules are indicated. The 3′-tailed substrates used in lanes 3–8 are as shown in Figures 1A and 4A. The 3′-tailed substrates used in lanes 1 and 2 is the same as shown in Figure 1A but includes 10-nt non-homologous to the dsDNA partner at the 3′-end. The circular dsDNA plasmids used were all the same length; lanes 1–4 used pDR6, lanes 5 and 6 used pDR5 and lanes 7 and 8 used pDR4. (**B**) The joint molecules, formed as in lanes 7 and 8 of (A), were treated with SphI before deproteinization. The cartoon shows the arrangement expected of two joint molecule products based on SFM images, left top and bottom. The arrangement expected if the two joint molecule products represent different extent of strand exchange is shown at the right, top and bottom. The SphI site would be protected in joint molecules where pairing occurred and RAD51 is bound along the homologous region 3′ of the heterology but cut in joint molecules paired only 5′ of the heterology. Products of the restriction enzyme protection assay were deproteinized and then resolved by agarose gel electrophoresis.

ssDNA and non-homologous dsDNA are apparently too transient or unstable to detect in our SFM experiments. In the joint molecule intermediates, the dsDNA involved in strand exchange is stretched to the same extent as simple dsDNA bound by RAD51, indicating that this DNA distortion is likely an intrinsic aspect of interaction with the recombinase filament even in these intermediates including three DNA strands.

We discovered and quantified several notable architectural features of RAD51 joint molecules. At the 3′ end of the invading ssDNA the recipient dsDNA had increased flexibility, indicating disruption of double-helix structure at this point. The combination of a RAD51-bound joint molecule and the increased flexibility of the dsDNA could target proteins specifically needed at this location. At the other end of the joined region, corresponding to the 5′ end

of the invading ssDNA, the dsDNA is sharply and distinctly bent to 90°. Recombination proteins that influence RAD51 filament stability (22) and control the outcome of recombination are likely to recognize these different architectural features of joint molecules. For instance, the 3′ end of the invading ssDNA needs to be further processed in several ways; this site may be recognized to initiate RAD51 filament disruption (18,23), the extension of the invading DNA by polymerases starts here (24,25) and second end capture occurs here also (26,27). The kink at the 5′-end of the invading DNA may be recognized by mediator proteins that remodel or disassemble RAD51 filaments. This DNA distortion would also be a point of control for branch migration possibly modulated by proteins such as RAD51AP1 and BLM (28–31).

We expect strand exchange to be coupled to changes in the architecture of RAD51–DNA complexes. Here, our SFM imaging allowed us to compare filament stability in different regions of the same complex. RAD51 bound to joint regions was less regular than RAD51 bound to dsDNA alone, indicating that the filament is more dynamic during strand exchange. In contrast, RAD51 bound to the joint region was more stable to disassembly than RAD51-bound dsDNA. Our joint molecule formation and strand exchange assays were quite efficient even in the absence of RPA. However, the absence of RPA may affect the stability of RAD51-bound to joined DNA regions. It was not technically possible to include RPA in the SFM imaging assay for RAD51 filament disassembly on mica. The influence of RPA on filament stability will have to be tested in different single-molecule assays. The relative stability of RAD51 bound to joint molecules supports the idea that disassembly of RAD51 from the product of recombination requires mediator proteins, such as RAD54, RAD54B or BACH1 (11,18,32–34).

RAD51 mediated homologous recombination can proceed through some sequence heterology, *in vivo* allowing similar but not identical sequences to recombine but is stringent enough to prevent rampant genome rearrangement. *In vitro* strand exchange by RAD51 can be blocked by >10 nt of heterologous sequence and is made less efficient by shorter stretches of heterology (35). In the absence of supercoiling, 10 nt of heterology blocked strand exchange at the stage of joint molecule extension. However, using linear DNA and a 4-nt heterologous substitution or a 10-nt substitution in supercoiled DNA, joint molecule extension often passed the heterology. There were no apparent changes in the architecture of bound RAD51 including the regions of heterology. In the structure of dsDNA-bound RecA only one strand of DNA contacts the proteins filament with the incoming recombination partner is held in place by Watson–Crick base pairing (6). Assuming the RAD51–DNA filament is similar, the absence of a difference in filament structure over mispaired bases suggests that they can be accommodated in the protein filament grove and the incoming strand held in placed by Watson–Crick base pairing distal to the mismatches.

Strand register may be lost as the region of heterology increases. Indeed when register is lost by a 4-nt insertions or deletions strand exchange by RecA is blocked, whereas 4-nt substitutions had little effect in an oligonucleotide based strand exchange assay (36). Consistent with what we show here for heterologous substitutions, strand exchange by yeast Rad51 is partially inhibited by 4-nt insertions or deletions and almost completely blocked with insertions or deletions >10 nt (35). Interestingly in that assay using ds linear and ss circular plasmid-size substrates (35), joint molecule intermediates were observed with heterologous insertions and deletions indicating partial strand exchange, similar to what we present here with heterologous substitutions.

Short stretches of heterology apparently slowed down strand exchange or causes instability in joint molecules. When 4 nt of heterology were encountered using linear substrates or 10 nt of heterology were encountered using supercoiled substrates, DNA pairing often occurred past the region of heterology but infrequently included the complete region of homology. Because the architecture of RAD51 filaments was the same on the joint molecules either at, or past, the region of heterology we favor the idea that an encounter with heterology delays otherwise normal joint molecule formation.

Together with the images of joint molecules, the gel assay provides intriguing clues to the effect of heterology on strand exchange. We observe two distinct strand exchange products in reactions with central heterologous sequences. One interpretation of these two products is that they migrate differently in the gel due to different arrangement of strands. This suggests that stable strand exchange does not require pairing of the 3′ ssDNA end. However, without more support this remains speculation. The more conventional interpretation is that the top band has undergone strand exchange across the complete region of ss DNA, just like the reactions without any heterology. The bottom band would then be due to less complete strand exchange. This is also a distinct band in the gel indicating that the extent of strand exchange was defined, perhaps stopping at the heterologous block. SFM images from the equivalent reaction mixture with supercoiled dsDNA, show joint molecules frequently extending past the position of heterology, to varying extents. It is possible that while joint molecules bypass the regions of heterology, stable strand exchange as detected in the gel did not.

Interestingly when joint molecule extension was blocked by heterologous sequences, about one-third of the intermediates we observed had paired with the 5′ half of the homologous ssDNA substrate and did not include the 3′-end, using both linear and circular dsDNAs. This suggests that initiation of strand exchange does not require an invading 3′ end. Pairing, and possible strand exchange, independent of a 3′-end would be important at stalled replication forks, where models for fork recovery show strand exchange steps involving template strands distal to stalled forks (37–39). Pairing on either side of a heterologous substitution is consistent with random collisions initiating strand exchange. The predominance of pairing between the heterology and 3′ ssDNA over pairing of the equally long 5′ ssDNA segments may be due to a number of factors specific to the DNA molecules used in this *in vitro* reaction. Most obviously, the 3′ end is

relatively unconstrained and could more rapidly sample for homology and for the same reason more easily initiate and proceed to a stable strand exchange intermediate.

Our observations of RAD51-mediated joint molecules provide mechanistic insight into several key steps of strand exchange. Open questions remain concerning the destabilizing role of heterology and how much heterology can be tolerated at different stages of strand exchange. The role of mediator proteins is also expected to modulate heterology tolerance. In addition, the control of filament disassembly in driving strand exchange forward and the role of accessory factors here remain to be defined.

SUPPLEMENTARY DATA

Supplementary Data are available at NAR Online.

ACKNOWLEDGEMENTS

We thank I. Pfeiffer, J. Lebbink and S.E. van Rossum-Fikkert for helpful comments on the manuscript and members of the Molecular Radiation Biology research group for valuable advice, support and help in all experimental efforts.

FUNDING

National Cancer Institute (USA) program project grant (SBDR 5PO1CA092584); Netherlands Organization for Scientific Research (NWO-Chemical Sciences-TOP); The Netherlands Genomic Initiative; C.W. is the recipient of an NWO-Chemical Sciences Vici award. Funding for open access charge: VICI grant 700.56.441 from Netherlands Organization for Scientific Research; Chemical Sciences (to C.W.).

Conflict of interest statement. None declared.

REFERENCES

1. Stasiak,A. and Di Capua,E. (1982) The helicity of DNA in complexes with recA protein. *Nature*, **299**, 185–186.
2. Griffith,J.D., Harris,L.D. and Register,J. III (1984) Visualization of SSB-ssDNA complexes active in the assembly of stable RecA-DNA filaments. *Cold Spring Harb. Symp. Quant. Biol.*, **49**, 553–559.
3. Ogawa,T., Yu,X., Shinohara,A. and Egelman,E.H. (1993) Similarity of the yeast RAD51 filament to the bacterial RecA filament. *Science*, **259**, 1896–1899.
4. Conway,A.B., Lynch,T.W., Zhang,Y., Fortin,G.S., Fung,C.W., Symington,L.S. and Rice,P.A. (2004) Crystal structure of a Rad51 filament. *Nat. Struct. Mol. Biol.*, **11**, 791–796.
5. VanLoock,M.S., Yu,X., Yang,S., Lai,A.L., Low,C., Campbell,M.J. and Egelman,E.H. (2003) ATP-mediated conformational changes in the RecA filament. *Structure*, **11**, 187–196.
6. Chen,Z., Yang,H. and Pavletich,N.P. (2008) Mechanism of homologous recombination from the RecA-ssDNA/dsDNA structures. *Nature*, **453**, 489–484.
7. Yu,X., VanLoock,M.S., Yang,S., Reese,J.T. and Egelman,E.H. (2004) What is the structure of the RecA-DNA filament? *Curr Protein Pept. Sci.*, **5**, 73–79.
8. Ristic,D., Modesti,M., van der Heijden,T., van Noort,J., Dekker,C., Kanaar,R. and Wyman,C. (2005) Human Rad51 filaments on double- and single-stranded DNA: correlating regular and irregular forms with recombination function. *Nucleic Acids Res.*, **33**, 3292–3302.
9. Modesti,M., Ristic,D., van der Heijden,T., Dekker,C., van Mameren,J., Peterman,E.J., Wuite,G.J., Kanaar,R. and Wyman,C. (2007) Fluorescent human RAD51 reveals multiple nucleation sites and filament segments tightly associated along a single DNA molecule. *Structure*, **15**, 599–609.
10. van der Heijden,T., Seidel,R., Modesti,M., Kanaar,R., Wyman,C. and Dekker,C. (2007) Real-time assembly and disassembly of human RAD51 filaments on individual DNA molecules. *Nucleic Acids Res.*, **35**, 5646–5657.
11. van Mameren,J., Modesti,M., Kanaar,R., Wyman,C., Peterman,E.J. and Wuite,G.J. (2009) Counting RAD51 proteins disassembling from nucleoprotein filaments under tension. *Nature*, **457**, 745–748.
12. Mine,J., Disseau,L., Takahashi,M., Cappello,G., Dutreix,M. and Viovy,J.L. (2007) Real-time measurements of the nucleation, growth and dissociation of single Rad51-DNA nucleoprotein filaments. *Nucleic Acids Res.*, **35**, 7171–7187.
13. Hilario,J., Amitani,I., Baskin,R.J. and Kowalczykowski,S.C. (2009) Direct imaging of human Rad51 nucleoprotein dynamics on individual DNA molecules. *Proc. Natl Acad. Sci. USA*, **106**, 361–368.
14. Liu,Y., Stasiak,A.Z., Masson,J.Y., McIlwraith,M.J., Stasiak,A. and West,S.C. (2004) Conformational changes modulate the activity of human RAD51 protein. *J. Mol. Biol.*, **337**, 817–827.
15. Bugreev,D.V. and Mazin,A.V. (2004) Ca2+ activates human homologous recombination protein Rad51 by modulating its ATPase activity. *Proc. Natl Acad. Sci. USA*, **101**, 9988–9993.
16. Yu,X., Jacobs,S.A., West,S.C., Ogawa,T. and Egelman,E.H. (2001) Domain structure and dynamics in the helical filaments formed by RecA and Rad51 on DNA. *Proc. Natl Acad. Sci. USA*, **98**, 8419–8424.
17. Benson,F.E., Stasiak,A. and West,S.C. (1994) Purification and characterization of the human Rad51 protein, an analogue of E.coli RecA. *EMBO J.*, **13**, 5764–5771.
18. Li,X., Zhang,X.P., Solinger,J.A., Kiianitsa,K., Yu,X., Egelman,E.H. and Heyer,W.D. (2007) Rad51 and Rad54 ATPase activities are both required to modulate Rad51-dsDNA filament dynamics. *Nucleic Acids Res.*, **35**, 4124–4140.
19. Brenner,S.L., Mitchell,R.S., Morrical,S.W., Neuendorf,S.K., Schutte,B.C. and Cox,M.M. (1987) recA protein-promoted ATP hydrolysis occurs throughout recA nucleoprotein filaments. *J. Biol. Chem.*, **262**, 4011–4016.
20. Garcia,R.A., Bustamante,C.J. and Reich,N.O. (1996) Sequence-specific recognition of cytosine C5 and adenine N6 DNA methyltransferases requires different deformations of DNA. *Proc. Natl Acad. Sci. USA*, **93**, 7618–7622.
21. Riddles,P.W. and Lehman,I.R. (1985) The formation of paranemic and plectonemic joints between DNA molecules by the recA and single-stranded DNA-binding proteins of Escherichia coli. *J. Biol. Chem.*, **260**, 165–169.
22. San Filippo,J., Sung,P. and Klein,H. (2008) Mechanism of eukaryotic homologous recombination. *Annu. Rev. Biochem.*, **77**, 229–257.
23. Sommers,J.A., Rawtani,N., Gupta,R., Bugreev,D.V., Mazin,A.V., Cantor,S.B. and Brosh,R.M. Jr (2009) FANCJ uses its motor ATPase to destabilize protein-DNA complexes, unwind triplexes, and inhibit RAD51 strand exchange. *J. Biol. Chem.*, **284**, 7505–7517.
24. McIlwraith,M.J., Vaisman,A., Liu,Y., Fanning,E., Woodgate,R. and West,S.C. (2005) Human DNA polymerase eta promotes DNA synthesis from strand invasion intermediates of homologous recombination. *Mol. Cell*, **20**, 783–792.
25. Li,X. and Heyer,W.D. (2009) RAD54 controls access to the invading 3'-OH end after RAD51-mediated DNA strand invasion in homologous recombination in Saccharomyces cerevisiae. *Nucleic Acids Res.*, **37**, 638–646.
26. McIlwraith,M.J. and West,S.C. (2008) DNA repair synthesis facilitates RAD52-mediated second-end capture during DSB repair. *Mol. Cell*, **29**, 510–516.

27. Nimonkar,A.V., Sica,R.A. and Kowalczykowski,S.C. (2009) Rad52 promotes second-end DNA capture in double-stranded break repair to form complement-stabilized joint molecules. *Proc. Natl Acad. Sci. USA*, **106**, 3077–3082.
28. Modesti,M., Budzowska,M., Baldeyron,C., Demmers,J.A., Ghirlando,R. and Kanaar,R. (2007) RAD51AP1 is a structure-specific DNA binding protein that stimulates joint molecule formation during RAD51-mediated homologous recombination. *Mol. Cell*, **28**, 468–481.
29. Wiese,C., Dray,E., Groesser,T., San Filippo,J., Shi,I., Collins,D.W., Tsai,M.S., Williams,G.J., Rydberg,B., Sung,P. *et al.* (2007) Promotion of homologous recombination and genomic stability by RAD51AP1 via RAD51 recombinase enhancement. *Mol. Cell*, **28**, 482–490.
30. Bugreev,D.V., Hanaoka,F. and Mazin,A.V. (2007) Rad54 dissociates homologous recombination intermediates by branch migration. *Nat. Struct. Mol. Biol.*, **14**, 746–753.
31. Bachrati,C.Z., Borts,R.H. and Hickson,I.D. (2006) Mobile D-loops are a preferred substrate for the Bloom's syndrome helicase. *Nucleic Acids Res.*, **34**, 2269–2279.
32. Wesoly,J., Agarwal,S., Sigurdsson,S., Bussen,W., Van Komen,S., Qin,J., van Steeg,H., van Benthem,J., Wassenaar,E., Baarends,W.M. *et al.* (2006) Differential contributions of mammalian Rad54 paralogs to recombination, DNA damage repair, and meiosis. *Mol. Cell. Biol.*, **26**, 976–989.
33. Chi,P., Kwon,Y., Seong,C., Epshtein,A., Lam,I., Sung,P. and Klein,H.L. (2006) Yeast recombination factor Rdh54 functionally interacts with the Rad51 recombinase and catalyzes Rad51 removal from DNA. *J. Biol. Chem.*, **281**, 26268–26279.
34. Prakash,R., Satory,D., Dray,E., Papusha,A., Scheller,J., Kramer,W., Krejci,L., Klein,H., Haber,J.E., Sung,P. *et al.* (2009) Yeast Mph1 helicase dissociates Rad51-made D-loops: implications for crossover control in mitotic recombination. *Genes Dev.*, **23**, 67–79.
35. Holmes,V.F., Benjamin,K.R., Crisona,N.J. and Cozzarelli,N.R. (2001) Bypass of heterology during strand transfer by Saccharomyces cerevisiae Rad51 protein. *Nucleic Acids Res.*, **29**, 5052–5057.
36. Bucka,A. and Stasiak,A. (2001) RecA-mediated strand exchange traverses substitutional heterologies more easily than deletions or insertions. *Nucleic Acids Res.*, **29**, 2464–2470.
37. Wyman,C. and Kanaar,R. (2006) DNA double-strand break repair: all's well that ends well. *Annu. Rev. Genet.*, **40**, 363–383.
38. Eppink,B., Wyman,C. and Kanaar,R. (2006) Multiple interlinked mechanisms to circumvent DNA replication roadblocks. *Exp. Cell. Res.*, **312**, 2660–2665.
39. Cox,M.M., Goodman,M.F., Kreuzer,K.N., Sherratt,D.J., Sandler,S.J. and Marians,K.J. (2000) The importance of repairing stalled replication forks. *Nature*, **404**, 37–41.